

Gaussian Process Assisted Meta-learning for Image Classification and Object Detection Models

Anna R. Flowers^{*†} Christopher T. Franck[†] Robert B. Gramacy[†] Justin A. Krometis^{‡§}

December 24, 2025

Abstract

Collecting operationally realistic data to inform machine learning models can be costly. Before collecting new data, it is helpful to understand where a model is deficient. For example, object detectors trained on images of rare objects may not be good at identification in poorly represented conditions. We offer a way of informing subsequent data acquisition to maximize model performance by leveraging the toolkit of computer experiments and metadata describing the circumstances under which the training data was collected (e.g., season, time of day, location). We do this by evaluating the learner as the training data is varied according to its metadata. A Gaussian process (GP) surrogate fit to that response surface can inform new data acquisitions. This meta-learning approach offers improvements to learner performance as compared to data with randomly selected metadata, which we illustrate on both classic learning examples, and on a motivating application involving the collection of aerial images in search of airplanes.

Keywords: computer experiment, metadata, data acquisition

1 Introduction

We consider scenarios where labeled data D_N are used to train a machine learning (ML) model (e.g., neural network (NN; Rosenblatt, 1958; Rumelhart et al., 1986), random forest (RF; Breiman, 2001), or support vector machine (Cortes and Vapnik, 1995)), but collecting and labeling data is the most expensive part of the process. Examples of such scenarios include medical imaging (Willemink et al., 2020; Hoi et al., 2006), natural language processing (Olsson, 2009), speech recognition (Abdelwahab and Busso, 2019), and streaming data (Žliobaitė et al., 2013; Zhu et al., 2007). In these scenarios, it is important to ensure that the data collected provides the ML model with as much information as possible. Consider, for example, collecting images used to train an image classifier. After training, the model will correctly classify some images and incorrectly classify others. Our goal is to identify the *types* of images the model categorizes accurately, or otherwise, in hopes of curating the composition of future image collection.

Selecting data with the goal of improving a model is called active learning (AL). The core idea behind AL is to choose new data points in an intelligent way so that model performance is as good as possible under stringent data budgets. There is an extensive literature of AL within the field of ML, which we refer

^{*}Corresponding author: arflowers@vt.edu

[†]Department of Statistics, Virginia Tech

[‡]Department of Mathematics, Virginia Tech

[§]Virginia Tech National Security Institute

to as ML-AL; for a full review of ML-AL see Settles (2009) or Ren et al. (2021). ML-AL typically assumes that unlabeled data is cheap, and that only labeling is expensive. The process may involve requesting labels for a chosen combination of inputs (membership query synthesis; Angluin, 1988) or for specific data points selected from a pool of unlabeled ones (stream- and pool-based sampling; Lewis, 1995; Dagan and Engelson, 1995), whereby they are subsequently labeled, say via uncertainty sampling (Lewis and Gale, 1994), expected model change (Settles et al., 2007; Roy and McCallum, 2001), diversity sampling (Brinker, 2003), query-by-committee (Seung et al., 1992), or hybrids thereof (Yang et al., 2015; Ash et al., 2019; Yin et al., 2017). Both options have drawbacks. Since the input space is complex for ML models, membership query synthesis may request a combination of inputs that is unrecognizable to the annotator, meaning it cannot be labeled (Baum and Lang, 1992). Stream- and pool-based sampling methods are far more common, but rely on the assumption that collecting unlabeled data is cheap and only the labeling is expensive. When collecting unlabeled data is also expensive, another AL method is needed.

Our idea is to select new data points according to their metadata. In this paper we define metadata as any feature of the data that is not available to the model during training. Since image classifiers, for example, are trained using only the pixels of images, any extra information about those images can be treated as metadata. We choose to select new data points in this way because we believe that data points with different metadata may yield different model performance. By choosing new data points according to their metadata, we learn the types of data points that are most useful to the model.

As an example, consider a motivating dataset known as RarePlanes (Shermeyer et al., 2021), a collection of 8,525 aerial images of 25,205 planes. RarePlanes contains many examples of metadata (e.g., weather, time of day, location). Exploring the relationship between these quantities and model performance in the RarePlanes dataset is not a new idea (Lanus et al., 2024; Torres et al., 2020); however, we are the first to frame this problem in an AL context. Here we focus on a metadata record indicating weather when the photo was taken: snowy, or not snowy. To see why data points with one type of weather metadata may be more valuable than another, see Figure 1. For now, consider only the box labeled D_N on the

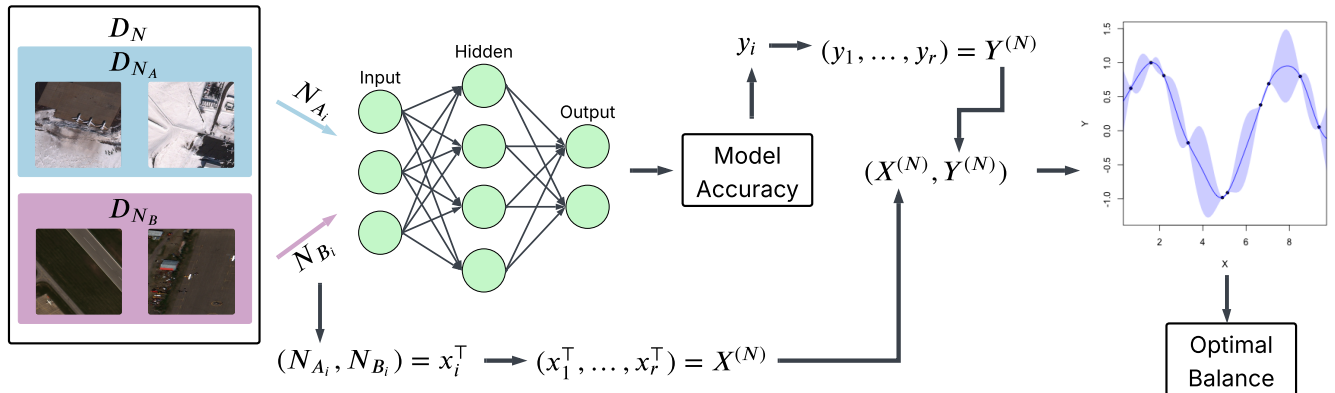


Figure 1: Process for identifying the optimal balance of metadata.

far left, representing the entire dataset. Inside this box are two smaller boxes, colored blue and pink, containing two images each. Blue and pink boxes represent two metadata categories; blue with snow, and pink without. Since many of the planes are white, they are harder to distinguish from the background in images with snow (verified in Appendix A.3). It is therefore harder for an ML object detector to accurately detect planes in images with snow than otherwise. However, what this means about ideal data for learning is not immediate. Harder to distinguish images may provide more information per data point, but they

risk decreasing predictive accuracy for images without snow, which may be more common in applications where the model is deployed.

Somewhat more generically, let A denote one metadata category (e.g., snow), and B denote its complement (not snow). Throughout this paper we consider only two metadata categories and discuss potential for more categories in our discussion at the end of the paper. These categories partition a full set of N training data records D_N into D_{N_A} and D_{N_B} . Our idea is to vary the metadata balance through N_A and N_B in order to explore the the accuracy of ML models fit to those data. This is represented in the middle of Figure 1 as N_{A_i} and N_{B_i} fed into NN (an example ML model). Each (N_{A_i}, N_{B_i}) , for $i = 1, \dots, r$ is saved in a vector $x_i^\top = (N_{A_i}, N_{B_i})$. Out-of-sample model accuracy under each x_i^\top , denoted as a_{N_i} (e.g., correct classification rate (CCR) or F1-score), and is saved as $y_i = a_{N_i}$.

The process of varying a metadata balance and recording its corresponding model accuracy is a computer experiment. Data comprised of r evaluations of this response surface, which we denote as $(X^{(N)}, Y^{(N)})$, can be used to fit a surrogate model (Santner et al., 2003; Gramacy, 2020) such as a Gaussian process (GP; Rasmussen and Williams, 2006). That surrogate can then be searched to determine advantageous input conditions x for learning, in this case determining an optimal metadata balance of future A and B images. This is shown as the final step of Figure 1. We refer to this process as GP-assisted meta-learning (GPAML). We believe we are the first to apply GP to a performance surface and then view things in a computer experiment context.

Although GPAML is a form of learning that leverages a GP, it is fundamentally different than typical GP active learning (GP-AL) methods. GP-AL methods seek to either improve (Seo et al., 2000; Cohn, 1993; MacKay, 1992) or optimize (Jones et al., 1998; Snoek et al., 2012; Picheny et al., 2016) the GP response surface itself, whereas GPAML uses the GP response surface to improve *future* ML model accuracy. Consequently GPAML is inherently extrapolative in nature, making it more like ML-AL, but aided by a GP. We intend to make this distinction clear as the development progresses. We also note that others have used the word meta-learning in similar contexts; for a review of others, see Vilalta and Drissi (2002) or Hospedales et al. (2021). Our work is also distinct from what is known as meta-active learning (e.g., Hsu and Lin, 2015; Fang et al., 2017; Konyushkova et al., 2017), referring to algorithms with flexible acquisition functions that are updated at each step of the active learning process.

The remainder of the paper is organized as follows. Section 2 contains our main methodological contribution: GPAML, after a brief review of GPs. Section 3 provides benchmarking results on three datasets, including the motivating RarePlanes dataset. Section 4 contains a short discussion of limitations and possible future work. All code is provided via Git: <https://bitbucket.org/gramacylab/metalearn>.

2 GP-Assisted Meta-learning

We begin with a brief review of GP surrogate modeling and then turn to our main contribution.

2.1 Gaussian Processes

Consider modeling r runs of a computer experiment using a GP (Sacks et al., 1989). Let $X = (x_1^\top, \dots, x_r^\top)$ be an $r \times p$ matrix of inputs, and $Y = (y_1, \dots, y_r)$ be a corresponding $r \times 1$ vector of outputs. A GP prior

implies $Y \sim \mathcal{N}_r(\mu(X), \Sigma(X))$, often with $\mu(X) = 0$ after centering. This induces the likelihood

$$L(Y | X) \propto |\Sigma(X)|^{-\frac{1}{2}} \exp\left(-\frac{1}{2} Y^\top \Sigma(X)^{-1} Y\right)$$

where $\Sigma(X)_{ij} = \Sigma(x_i, x_j) = \tau^2 \left(\exp\left(-\frac{\|x_i - x_j\|^2}{\theta}\right) + g \mathbb{I}_{\{i=j\}} \right)$.

Although other *kernels* defining $\Sigma(X)$ are common (e.g., Abrahamsen, 1997; Stein, 1999), we prefer a simple squared exponential form. Hyperparameters τ^2 , θ , and g represent the scale, lengthscale, and noise, respectively, and may be inferred via maximum likelihood (MLE).

Conditional on data (X, Y) and hyperparameters τ^2 , θ , and g , predictions can be made for an $r' \times p$ matrix $\mathcal{X} = (\tilde{x}_1^\top, \dots, \tilde{x}_{r'}^\top)$ of new inputs. Gaussian conditioning gives $Y(\mathcal{X}) | X, Y \sim \mathcal{N}_{r'}(\mu_{\mathcal{X}}, \Sigma_{\mathcal{X}})$, where

$$\mu_{\mathcal{X}} = \Sigma(\mathcal{X}, X) \Sigma(X)^{-1} Y, \quad \text{using } \Sigma(\mathcal{X}, X)_{ij} = \Sigma(\tilde{x}_i, x_j),$$

and $\Sigma_{\mathcal{X}} = \Sigma(\mathcal{X}) - \Sigma(\mathcal{X}, X) \Sigma(X)^{-1} \Sigma(\mathcal{X}, X)^\top$.

As shorthand, we use $\text{GP}(\mathcal{X}; X, Y)$ to refer to predictions made by a GP at \mathcal{X} following these equations using MLE hyperparameters. Deriving such a surface represents the final step of GPAML; refer to Figure 1. Since it is trained on model accuracy for varying metadata composition, we shall refer to $\text{GP}(\mathcal{X}; X, Y)$ as an “accuracy surface” in this paper.

2.2 An experiment varying the metadata balance

Consider a collection of N pairs of data points and their labels $D_N = ((d_1, \ell_1), \dots, (d_N, \ell_N))$ and a holdout set $H_{N'} = ((d'_1, \ell'_1), \dots, (d'_{N'}, \ell'_{N'}))$ of N' new data points and their labels. In the case of image classification, d_i is the pixel array for the i^{th} image and ℓ_i is the corresponding classification label. Suppose that D_N and $H_{N'}$ have been used to train and evaluate, respectively, a ML model $\text{ML}(H_{N'}; D_N)$, e.g., as described in Section 1, producing model accuracy a_N . Our goal is to use D_N , but not $H_{N'}$, to decide on what n new data points and labels to add to D_N , and then re-train/evaluate $\text{ML}(H_{N'}; D_{N+n})$. Because both collecting data points and then labeling them is expensive, we want to ensure that the n new data points collected are useful to the model. Useful is defined as data which produce the best values of a_{N+n} , the new model accuracy. We exploit metadata information to learn optimally useful new data points. Since we consider only two metadata categories in this work, A and B partitioning D_N , choosing n new points is equivalent to determining the proportion or amount belonging to either category, n_A or $n_B = n - n_A$.

Now, consider an experiment designed to create many different sub-datasets sampled from D_N via D_{N_A} and D_{N_B} , each with different metadata balances for training, along with hold-out sets for testing so that accuracy can be measured for each metadata balance. Focus on a single repetition or instance i of this experiment. Begin by sampling a random number of images from each metadata category. More explicitly, sample two random integers N_{A_i} and N_{B_i} representing the number of data points to select from each category in rep i . Ideally, N_{A_i} is a random integer between 1 and N_A , and N_{B_i} is a random integer between 1 and N_B . In practice, the number of points available for training is less than N_A and N_B because some points must be reserved testing; details on how the test set is selected are provided in the next few paragraphs. Once the values of N_{A_i} and N_{B_i} have been selected, use those values to sample datasets $D_{N_{A_i}} = \text{samp}(D_{N_A}, N_{A_i})$ and $D_{N_{B_i}} = \text{samp}(D_{N_B}, N_{B_i})$, where $\text{samp}(D, N)$ indicates randomly selecting N images from dataset D . Combine these into $D_{N_i} = (D_{N_{A_i}}, D_{N_{B_i}})$, and use D_{N_i} to train the ML model.

After selection and training with D_{N_i} , we must evaluate the performance of the ML model out-of-

sample. That is, we must compute accuracy a_{N_i} for some test set $D_{N_i}^{\text{test}}$. The decision of how to compose $D_{N_i}^{\text{test}}$ is nontrivial because model accuracy a_{N_i} changes depending on $D_{N_i}^{\text{test}}$, affecting our accuracy response surface that ultimately chooses the optimal balance of new test points (n_A, n_B) . More on this in Section 2.4. In particular, if $D_{N_i}^{\text{test}}$ is not similar, in terms of proportion balance in each metadata category A and B , to the true proportion balance, any downstream decision making may not generalize well.

Here we assume to know, or that we can estimate, the population proportion balance, denoted (p_A^0, p_B^0) . This guides our choice of random testing set, separately for each rep i . Somewhat arbitrarily, but we think also sensibly, we choose 10% of D_N for $D_{N_i}^{\text{test}}$, meaning the metadata (count) balance of $D_{N_i}^{\text{test}}$ is $(0.1Np_A^0, 0.1Np_B^0)$. This restricts the upper bounds for N_{A_i} and N_{B_i} for training. Specifically, to ensure $D_{N_i} \cap D_{N_i}^{\text{test}} = \emptyset$, we sample N_{A_i} between 1 and $N - 0.1Np_A^0$, and N_{B_i} between 1 and $N - 0.1Np_B^0$. Given $D_{N_i}^{\text{test}}$, and $D_{N_i} = (D_{N_{A_i}}, D_{N_{B_i}})$ so constructed, and out of sample accuracy $y_i = a_{N_i}$ associated with metadata balance $x_i^\top = (N_{A_i}, N_{B_i})$ estimated, the subsampling process may be repeated for $i = 1, \dots, r$ to get $X^{(N)} = (x_1^\top, \dots, x_r^\top)$ and $Y^{(N)} = (y_1, \dots, y_r)$. The (N) superscript denotes that sub-samples were collected from D_N . We will use $(X^{(N)}, Y^{(N)})$ in Section 2.4 to train a GP and produce an accuracy surface.

For each unique metadata balance pair, there are many subsamples of data points that could be selected from D_{N_A} and D_{N_B} . In particular, for a given N_A , N_B , N_{A_i} , and N_{B_i} , there are $\binom{N_A}{N_{A_i}} \binom{N_B}{N_{B_i}}$ possible combinations. Each subsample will yield a different model accuracy. Therefore, we do not sample r unique metadata balance pairs, but rather choose to *block* the experiment by a smaller number b unique metadata balance pairs, along with z “replicates” so that $r = bz$. This helps with separating signal from noise when fitting the GP surrogate; more in Section 2.4. Algorithm 1 summarizes this subsampling process.

Algorithm 1 Experiment varying the metadata balance

Require: $N, N_A, N_B, p_A^0, p_B^0, b, z$

- 1: **for** $j \in 1, \dots, b$ **do**
- 2: $N_{A_j} \sim \mathcal{U}(1, N_A - 0.1Np_A^0)$ ▷ sample counts for training set
- 3: $N_{B_j} \sim \mathcal{U}(1, N_B - 0.1Np_B^0)$
- 4: **for** $k \in 1, \dots, z$ **do**
- 5: $D_{N_{A_{jk}}}^{\text{test}} = \text{samp}(D_{N_A}, 0.1Np_A^0)$ ▷ collect test sets
- 6: $D_{N_{B_{jk}}}^{\text{test}} = \text{samp}(D_{N_B}, 0.1Np_B^0)$
- 7: $D_{N_{A_{jk}}} = \text{samp}(D_{N_A} \setminus D_{N_{A_{jk}}}^{\text{test}}, N_{A_j})$ ▷ collect training sets
- 8: $D_{N_{B_{jk}}} = \text{samp}(D_{N_B} \setminus D_{N_{B_{jk}}}^{\text{test}}, N_{B_j})$
- 9: $x_{b(j-1)+k} = (N_{A_j}, N_{B_j}); y_{b(j-1)+k} = \text{ML}(D_{N_{jk}}^{\text{test}}; D_{N_{jk}})$ ▷ run ML model and save performance
- 10: **end for**
- 11: **end for**
- 12: $X^{(N)} = (x_1^\top, \dots, x_{bz}^\top)$ ▷ combine data from all iterations
- 13: $Y^{(N)} = (y_1, \dots, y_{bz})$

$\mathcal{U}(a, b)$ in lines 2 and 3 refers to a sample from a discrete uniform distribution over $\{a, a + 1, \dots, b\}$.

2.3 Conic meta-learning

We now present an idea for meta-learning, called conic meta-learning, that can be used for any accuracy (response) surface. We first use an arbitrary surface to describe the meta-learning approach for adaptively adding data, ignoring the ML model and corresponding surrogate fit to simplify the experiment. We return to actual meta-learning with a GP in Section 2.4. For now, imagine an accuracy surface trained on data

$(X^{(N)}, Y^{(N)})$, where $X^{(N)}$ and $Y^{(N)}$ have the same meaning as in Section 2.2, except that they follow

$$y_i \sim \mathcal{N}(f(x_1, x_2), 0.05^2), \quad \text{where} \quad f(x_1, x_2) = 1 - \exp\left(-\frac{x_1 x_2}{10x_1 + 15x_2}\right), \quad (1)$$

and x_1 and x_2 represent the number of data points subsampled from category A and category B , respectively (i.e., values of N_{A_i} and N_{B_i}). Data simulated from the process (1) have important qualities as relates to our actual meta-learning application: (i) the mean function is monotonic in each dimension and (ii) the response y_i is noisy. Monotonicity is important because ML models generally get more accurate as more data is added; noise is important since controlling metadata does not pin down the actual training/testing examples in the partition, which is our reason for blocking in Algorithm 1.

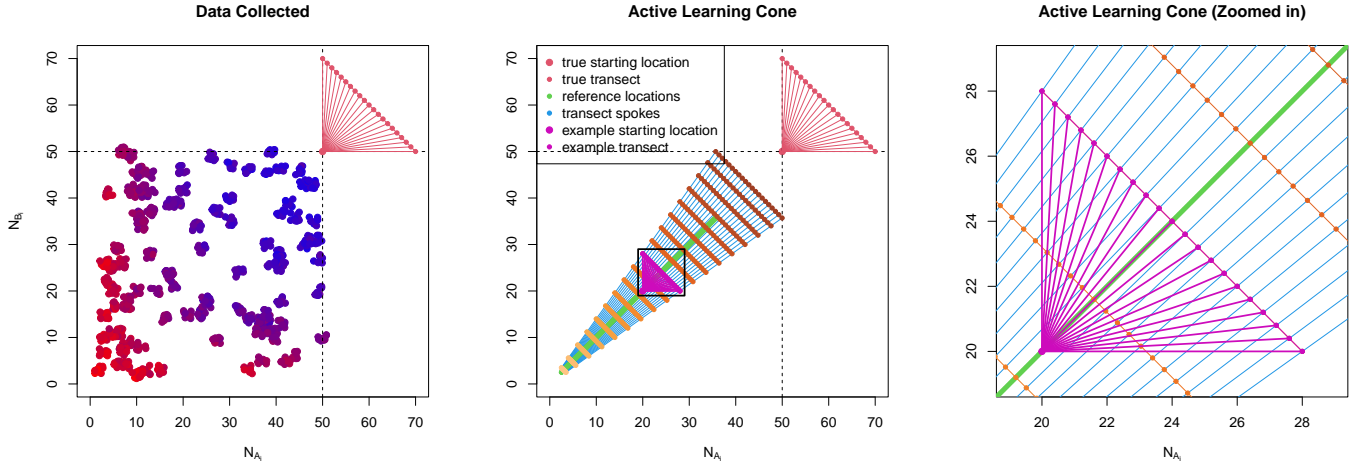


Figure 2: *Left:* Sample data points $X^{(N)}$, colored by value of $Y^{(N)}$. *Center:* Cone resulting from all possible reference locations. *Right:* Center plot, zoomed in to boxed region. This shows all possible paths for the reference location $(20, 20)$.

The left panel of Figure 2 provides an example/representative dataset following Eq. (1). The x - and y -coordinates on the plot represent x_1 and x_2 , or metadata categories A and B , and the color of each dot indicates the level of y . Colors closer to blue have higher model accuracy, and colors closer to red have lower model accuracy. Clusters of points on the plot come from replicates in the blocked design, shown with jitter to see all values of y in the block. For this example we assume $N = 100$, $N_A = N_B = 50$, and that we wish to add $n = 20$ new points. The true starting metadata balance in D_N is $(N_A, N_B) = (50, 50)$ and is indicated as a red dot.

When starting with a balance of $(50, 50)$ and adding $n = 20$ new points, there are exactly 21 ways new points (n_A, n_B) can be added with respect to the metadata category balances: $((0, 20), (1, 19), \dots, (20, 0))$. By adding each of these 21 possible new point configurations to our current metadata balance $(50, 50)$, we get a *transect matrix* $T = ((50, 70)^\top, (51, 69)^\top, \dots, (70, 50)^\top)$ of new possible metadata balances. In the middle panel of the figure, lines connecting the starting balance $(50, 50)$ to each point of the transect are shown in red, representing the 21 possible ‘‘paths’’ of meta-learning. Our goal is to choose the path which provides the best model accuracy.

To choose the best meta-learning path, we use the accuracy surface created by training a model on $(X^{(N)}, Y^{(N)})$. Notice in the left two panels of Figure 2 that all samples in $(X^{(N)}, Y^{(N)})$ are bounded by 50 in both dimensions, emphasized using the dashed lines. This is because we only have 50 data points from each category to choose from (i.e., starting metadata balance $(50, 50)$). Therefore, the predictions in

the accuracy surface are only reliable inside the dashed lines. This is a problem, because the data points of interest (the transect T), lie outside of the bounds of the model (i.e., we are trying to extrapolate). We need a way to connect the data points in T to data points in the accuracy surface so that we can use the accuracy surface to make a decision. Our key assumption in this paper is that the behavior of the accuracy surface is roughly stationary with regards to proportion balance. In other words, that we may use data points with the same proportion balance as T , but with smaller N_{A_i} and N_{B_i} , to decide on acquisitions.

Consider representing the metadata balance as a proportion instead of a count. The true metadata balance $(50, 50)$ has a corresponding proportion balance $(\frac{N_A}{N} = \frac{1}{2}, \frac{N_B}{N} = \frac{1}{2})$. Within the range of the accuracy surface, we have many data points showing model performance when the proportion balance is $(\frac{1}{2}, \frac{1}{2})$; one example is at $(20, 20)$. If we were to visualize all data points with this proportion balance, we would have a line at $y = \frac{N_B}{N_A}x$. This line is shown in green in middle and right panels of Figure 2. We refer to the points similar to $(50, 50)$ as reference locations $R_q = \text{ref}(\frac{N_A}{N}, \frac{N_B}{N}, q)$, where q is the number of reference locations. The notation $\text{ref}(\frac{N_A}{N}, \frac{N_B}{N}, q)$ represents a matrix of q reference locations with the proportion balance $(\frac{N_A}{N}, \frac{N_B}{N})$, where each reference location is saved in a separate row. Our stationarity assumption means that model performance of the reference locations are representative of performance near (N_A, N_B) , and beyond for $(N_A + n_A, N_B + n_b)$.

Now that we have points similar to the true metadata balance, we wish to parlay that into transects similar to T . In other words, we want to find the transect T_j^{ref} corresponding to each reference location R_j , say in a grid indexed by $j = 1, \dots, q$. To show how to find these transects, consider a single reference location $(20, 20)$. This location is shown in pink in the right two panels of the figure; the right panel is zoomed in on the box highlighted in the center panel. To find a transect with respect to $(20, 20)$ that is representative of the transect with respect to $(50, 50)$, consider starting at $(20, 20)$ and creating paths that are “equivalent” to the paths starting at $(50, 50)$. Equivalent paths are defined as those which have the same percentage change in points as the true location. In our example, we are adding $n = 20$ new points to a dataset of size $N = 100$, which is a 20% increase in the size of the dataset. To add an equivalent number of points to the $(20, 20)$ reference location, we would add $0.2 \times 40 = 8$ new points. Adding an equivalent number of points can yield fractional points along the transect, but this is okay since a surrogate would approximate the entire response surface, not just integer inputs. For the $(20, 20)$ reference location, the transect would be $T_i^{\text{ref}} = ((20, 28)^\top, (20.2, 27.8)^\top, \dots, (28, 20)^\top)$. By adding new points according the percentage increase in size, the 21 points along each reference location’s transect have the same ending proportion balances as the original transect T .

The same process can be repeated for a dense sequence of reference locations (the green line in Figure 2). The complete array T^{ref} is a 3D array of length $j = 1, \dots, q$, where each entry is a 21×2 transect matrix. Lines connecting the 21 points of each transect are shown in blue. There are also many transects which are highlighted in shades of orange; these will be used to connect the visual to other plots in the next subsection where we shall look at the value of the accuracy surface at all of the points in all of the transects. Because we want to ensure these predictions are valid, we ensure that all transects are bounded by the model. We do this by only considering reference locations corresponding to transects that are bounded by the dashed lines. In particular, notice that the blue lines of the cone are all bounded by the dashed lines. The collection of all transects is conic in structure when plotted. For this reason, we refer to meta-learning done using this process as conic meta-learning.

2.4 Learning the optimal metadata balance

Now that we have a collection of transects T^{ref} corresponding to a collection of reference locations R_q , we want to combine the transects in such a way that we find the single optimal metadata balance. To do that,

we must incorporate a surrogate model into our example problem. Using the example data we explored in Section 2.3, we fit a GP trained on data $(X^{(N)}, Y^{(N)})$ to get the accuracy surface. The accuracy surface we are using is shown in the left panel of Figure 3 with the cone constructed in Section 2.3 overlaid. Only the

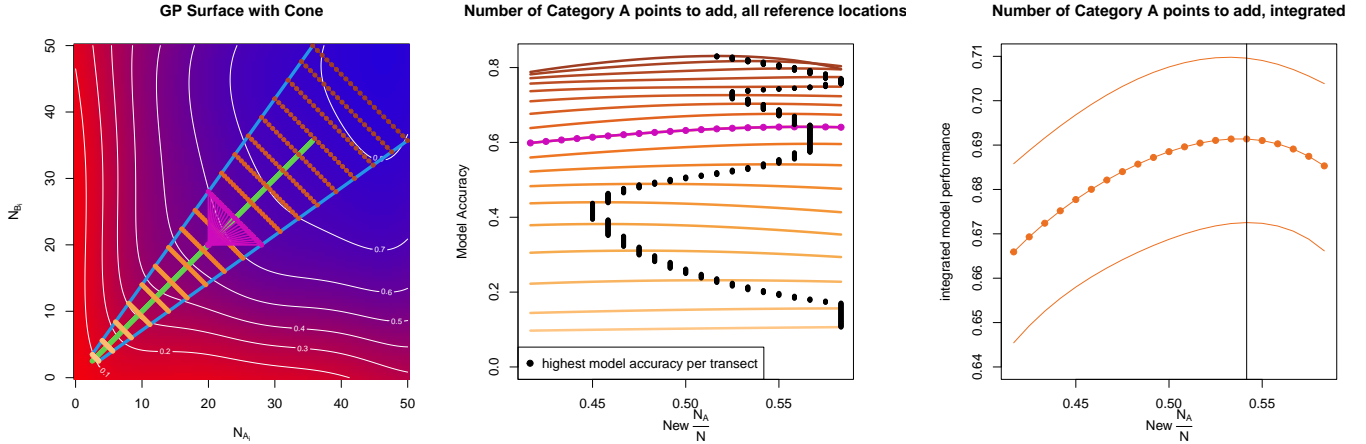


Figure 3: *Left:* GP surface with cone overlaid. *Center:* Transects of cone plotted against model performance. *Right:* Integrated model performance.

outside edges of the cone are shown for visual simplicity. In this plot, colors represent predicted accuracy at each location; locations that are more red have lower model accuracy and locations that are more blue have higher model accuracy. The contours in white show the same information. Notice again that the mean surface is monotonic in each dimension, since the model performs better on average as more data is added. The predicted accuracy at each input combination will be important for understanding the next step of the meta-learning process.

We now use the GP to predict the model accuracy for all transects, $\text{GP}(T^{\text{ref}}; X^{(N)}, Y^{(N)})$, saving the mean prediction in \mathcal{Y} . Recall that T^{ref} is an array, with each entry T_i^{ref} comprising of a single 21×2 transect matrix. Predictions are made at each entry T_i^{ref} separately, and for each entry the mean prediction is a vector of length 21. Doing this for all transects T^{ref} produces q vectors of length 21, which are saved in a $21 \times q$ matrix. In this way, each row of \mathcal{Y} represents a single ending proportion balance.

The center panel of Figure 3 offers a visual. Orange lines in this plot correspond to orange lines in the cone in the left panel; i.e., each line represents a transect. As before, the (20, 20) transect is shown in pink for reference. The center panel plots the ending proportion balance (with respect to Category A) associated with each of the 21 points in the transect against the predicted mean accuracy. Each orange line in the plot is a single column of \mathcal{Y} , where the x -axis is related to the entry number and the y -axis is the entry of that column. Across all columns, observations with the same entry number have the same ending proportion balance, indicated on the x -axis of the plot. For each transect, one of the 21 entries provides the maximum model accuracy. We show the entry with the best model accuracy for each transect as a black dot. This represents the optimal proportion balance for that transect. Note that every transect does not suggest the same optimal proportion balance.

The final step of this meta-learning process is to collapse \mathcal{Y} into a single piece of information. We know that each column of \mathcal{Y} suggests a single optimal proportion balance, but that the optimal proportion balance is different for each column. We propose collapsing \mathcal{Y} into a single column by computing a weighted average over the columns. In particular, we compute $G = \mathcal{Y}w$ to get a single vector G with 21 entries. Weights w are chosen such that more weight is given to transects in the upper right hand corner of the plot, because they are the most similar to the true transect T . We use linear weighting, but other approaches

could be used to adjust the impact of transects further from the starting balance (i.e., the transects closer to the bottom left corner of the accuracy surface). The resulting vector G is plotted in the right panel of Figure 3, with respect to Category A. The proportion balance associated with the entry number of G is on the x -axis, and the entry of G (the averaged model accuracy) is on the y -axis.

The proportion balance that produces the best value of G serves as our acquisition choice, i.e., $(n_A, n_B) = \arg \max_T(G)$. The optimally chosen proportion balance from our running example is shown as a vertical line in the right panel of Figure 3. Here, we learn that the optimal new proportion balance is $(\frac{65}{120}, \frac{55}{120})$, associated with transect entry $(65, 55)$, yielding $(n_A, n_B) = (15, 5)$. An algorithm detailing the steps explained in Sections 2.3 and 2.4 is shown in Algorithm 2, shorthanded as GPAML.

Algorithm 2 GPAML

Require: $X^{(N)}, Y^{(N)}, N, N_A, N_B, n, f, w$

- 1: Complete Algorithm 1.
- 2: $R_q = \text{ref}(\frac{N_A}{N}, \frac{N_B}{N}, q)$ ▷ create a sequence of q reference locations
- 3: $T = ((N_A + n, N_B)^\top, (N_A + n - 1, N_B + 1)^\top, \dots, (N_A, N_B + n)^\top)$ ▷ create transect matrix
- 4: **for** $i \in 1, \dots, q$ **do**
- 5: $n_{\text{ref}} = \frac{\sum R_{q_i}}{N}$ ▷ find equivalent move size for reference location
- 6: $T_i^{\text{ref}} = n_{\text{ref}} T$ ▷ get transect for reference location i
- 7: **end for**
- 8: $\mathcal{Y} = \text{GP}(T^{\text{ref}}; X^{(N)}, Y^{(N)})$ ▷ make GP predictions at reference location transects
- 9: $G = \mathcal{Y}w$ ▷ take weighted average of GP predictions
- 10: $(n_A, n_B) = \arg \max_T(G)$ ▷ choose (n_A, n_B) which optimizes G

GPAML can be completed many times in a row to make many consecutive batches of data acquisition, starting at data size N_{start} and ending at data size N_{stop} . We present a graphic in Figure 4 showing what this looks like in the context of GPAML. In this plot, the box labeled “Figure 1” refers to the process

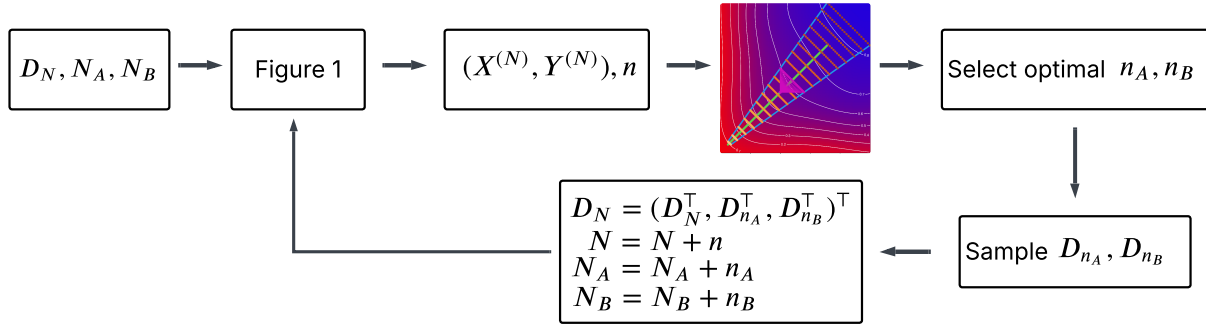


Figure 4: Multi-step GPAML, iterating over data sizes $N = N_{\text{start}}, \dots, N_{\text{stop}}$.

shown in Figure 1 up to the creation of $(X^{(N)}, Y^{(N)})$. The next panel, the GP surface with cone overlaid, represents using a GP surface to perform conic meta-learning. After using GPAML to select the optimal balance (n_A, n_B) and collect new data points accordingly, they are appended to the existing data. The new dataset D_N can be used for data subsampling, and the whole process can be repeated indefinitely. This allows researchers to continue collecting data until “enough” data has been collected. The question of when to stop collecting data is determined by a given problem’s budget and other constraints. Our multi-step GPAML approach guides data collection choices for the allocated budget.

3 Implementation and results

Here we present three examples to demonstrate the effectiveness of GPAML. A summary of each dataset/experiment is included in Table 1, with further details in subsections to follow. For each experiment we consider an

Dataset	ML Model	N_{start}	N_{stop}	n	Metadata	Reps	Perf. Criterion
Spambase	RF	100	500	20	Char/No char	100	CCR
MNIST	LeNet-5	100	200	20	Easy/hard	100	CCR
RarePlanes	YOLOv8	100	1000	50	Snow/Not snow	3	F1 Score

Table 1: Implementation information for each dataset/experiment.

initial dataset of size N_{start} , and add n new data points at a time until reaching size N_{stop} . At each size of the experiment N we evaluate out-of-sample (OOS) model performance with a holdout set $H_{N'}$ of size $N' = 1000$. Model performance is evaluated using either correct classification rate $\text{CCR} = \frac{\text{TP} + \text{TN}}{\text{TP} + \text{FN} + \text{TN} + \text{FN}}$ or F1 score $\text{F1} = \frac{\text{TP}}{\text{TP} + \frac{1}{2}(\text{FP} + \text{FN})}$, where TP, FN, TN, and FN represent the number of true positives, false negatives, true negatives, and false negatives, respectively. For each experiment the GP is trained on $r = 1000$ reps at $b = 100$ unique metadata balances. We consider three competing methods for data acquisition in our benchmarking exercises:

- **GPAML**: Our method as described in Section 2.
- **Random**: New data points are selected at random from a repository of data points.
- **Random Action**: The new metadata balance (n_A, n_B) is chosen at random.

All experiments were hosted in R, with NN models run in python. Code is provided at <https://bitbucket.org/gramacylab/metalearn>. We use the `RcppAlgos` (Wood, 2024) package to generate the transect vector T , and the `mleHomGP()` function in the `hetGP` (Binois and Gramacy, 2021) package with default settings to fit the GP.

3.1 Spambase

The first dataset we consider is the Spambase dataset (Hopkins and Suermondt, 1999), which summarizes a collection of 4,601 emails. It contains a total of 57 input variables describing features of the emails, and one output variable classifying the email as spam or non-spam. The input variables measure the frequency of certain words, numbers, special characters, and capital letters in the email.

There is technically no metadata provided with the dataset, so we engineered metadata categories for this experiment. We combined variables describing the frequency of specific special characters into one metadata variable describing the presence or absence of special characters in an email, and then removed the original variables as predictors available for training. So we have two metadata categories: A , emails with no special characters; and B , emails with at least one special character. We chose this metadata among other possibilities because exploratory analysis revealed that changing the distribution of special character/no special character emails affected ML model performance; see Appendix A.1.

For this experiment we started with $N_{\text{start}} = 100$ emails, adding $n = 20$ data points at a time until reaching size $N_{\text{stop}} = 500$. At each rep of the experiment, we choose a random number between 20 and 80 to represent the starting number of emails with at least one special character. This prevents choosing a starting metadata balance that would make GPAML infeasible (i.e., a very unbalanced dataset; we discuss

this further in Section 4). We use CCR to measure model accuracy. We use a random forest (RF) as our ML model and utilize the `randomForest` (Liaw and Wiener, 2002) package.

Out-of-sample CCR, averaged over 100 reps, is shown in the left panel of Figure 5. We provide mean

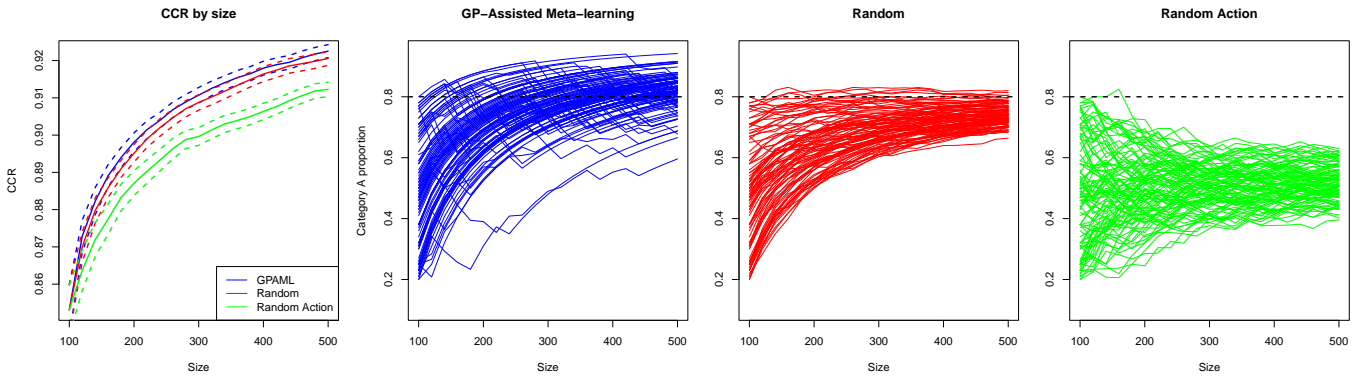


Figure 5: *Left:* OOS performance for each of the three methods. Proportion balances for GPAML (*center left*), random (*center right*), and random action (*right*) for each rep of experiment.

CCR and 95% confidence bounds for each of the three methods. Observe that GPAML performs as well or better than both of the competitor methods, in particular over the random action method. Although it does not perform much better than the random method, that is not necessarily a bad thing. Sampling new emails completely at random is not a realistic AL approach since we do not typically have access to the entire repository of data. In many cases, random selection is approximately optimal; we will discuss this further in Section 4. What is important is that GPAML has protected us from making a data acquisition that hurts model performance.

In the right three panels of Figure 5 we show the proportion balance for each rep of the experiment for each of the three methods, with proportion shown with respect to the character category. We also show a dashed line at $x = 0.8$, which is the true balance of special character/no special character emails, for reference. First notice that the random and random action methods converge to proportion balances of 0.8 and 0.5, respectively. Then notice that GPAML also converges roughly to a proportion balance of 0.8, more quickly but with higher variability than the random method. This indicates that the optimal proportion balance may vary slightly from one random training/testing partition to another. This is a strength of GPAML, since other methods of data acquisition do not consider the optimal proportion balance.

3.2 MNIST

The next dataset we consider is the Modified National Institute of Standards and Technology (MNIST) handwritten digit database (LeCun, 1998). This is a collection of 60,000 images of handwritten digits from 0-9. The dataset is widely available; we accessed it using the `dslabs` (Irizarry and Gill, 2024) R package. An LeNet-5 (LeCun et al., 1998) NN architecture was used for the ML model, leveraging the PyTorch (Paszke et al., 2019) package, and CCR was used to evaluate out-of-sample accuracy. Again, there is no freely available metadata, so we engineer metadata categories. Based on preprocessing, we binned each of the ten digits into digits that are easy to categorize and digits that are difficult to categorize. The digits in the easy, A category are 0, 1, 4, 5, 6, and 7 and the digits in the hard, B category are 2, 3, 8, and 9; see Appendix A.2 to see how these categories were chosen.

For this experiment we began with $N_{\text{start}} = 100$ images, adding $n = 20$ new images at a time until reaching size $N_{\text{stop}} = 200$. For a single rep of the experiment, we choose a random starting number of easy

images between 20 and 80. Results of this experiment, averaged over 100 reps, are shown in the left panel of Figure 6 via mean CCR and 95% confidence bounds for each of the three methods. Again, notice that

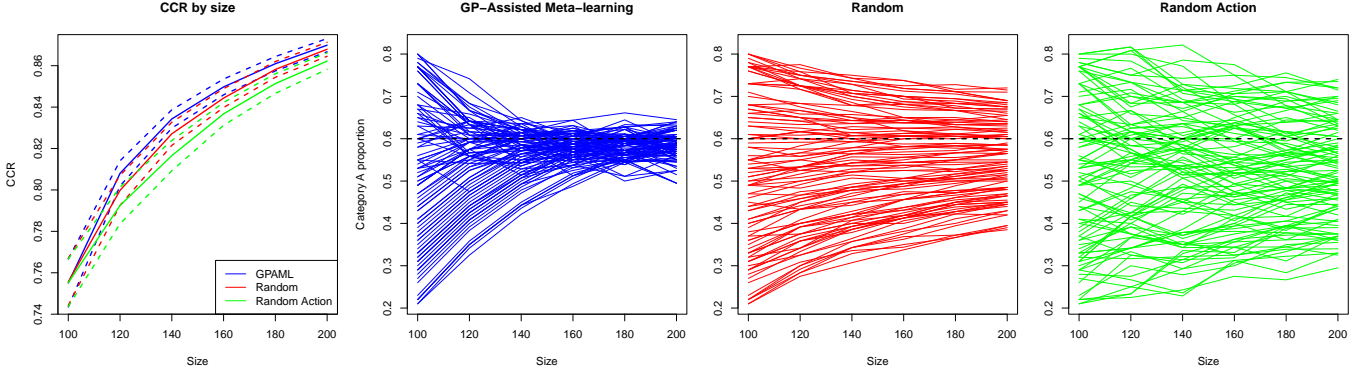


Figure 6: *Left:* OOS performance for each of the three methods. Proportion balances for GPAML (*center left*), random (*center right*), and random action (*right*) for each rep of experiment.

GPAML performs as well or better than both of the competitor methods, particularly random action. This is most evident from sizes $N = 120$ to $N = 160$ of the experiment; by size $N = 200$, random has caught up to GPAML.

The other three panels of the figure show overall proportion balance at each step of the meta-learning process. The proportion balance of each rep for GPAML, random, and random action is shown in the right three panels of Figure 6. The proportion balance is shown with respect to the easy category. We also include a dashed line at $y = 0.6$ to represent the true metadata balance of easy and hard digits. For this experiment, the random method converges to a balance of 0.6, and random action converges to a proportion of 0.5. The optimal proportion balance selected by GPAML is much more consistent in this case than with the Spambase data. In particular, there appears to be a narrow range of optimal proportion balances, ranging from about 0.55 to 0.65. What is interesting here is that GPAML quickly identifies that optimal proportion balance, and converges to it more quickly than either competitor.

3.3 RarePlanes

The final dataset we consider is our motivating example, the RarePlanes data (Shermeyer et al., 2021). This is a collection of 8,525 aerial images of planes. The RarePlanes dataset contains many forms of metadata, but we limit our focus to metadata describing the weather; we show that this metadata is suitable for our experiment in Appendix A.3. In the original RarePlanes dataset, this is divided into three categories: Clear Skies, Cloud Cover or Haze, and Snow. For simplicity, we combine the first two categories into a single category, Not Snow. YOLOV8 (Redmon et al., 2016; Ultralytics, 2023) is used for the ML model. YOLOV8 requires a user-specified validation set to use during model training. We sample a validation set of size $0.1N$, independent of D_{N_i} . For the purposes of training the GP, we treat any image in the validation set as part of the training set; i.e., the values of N_{A_i} and N_{B_i} include images in the validation set.

It is not immediately obvious why we would want to utilize GPAML for this dataset. Although here we have immediate access to all data points, in the real world we would need to manually collect data at each step of the active learning process. In particular, for each new data acquisition, we would need to collect new aerial images. This requires launching an airplane to capture the images. This is very expensive, since each launch requires people, gas, and time. This could even require a flight into hostile territory, meaning we want to collect data as efficiently as possible.

This experiment is very computationally intensive. YOLOV8 requires GPUs, and even when using those GPUs each model fit is slow. On average, each ML model training took around 30 minutes for the smallest sample size, and 4 hours for the largest sample size; in the previous two experiments model training took fewer than 5 seconds. Without parallelization, one rep of the experiment would take over two months to run. Note that this two month figure assumes resources are available for the duration of the experiment. Since we ran this experiment on a shared supercomputing cluster, we often had to wait for resources to become available, increasing the time needed to run the experiment. Therefore, even after parallelization each rep of the experiment takes around a month to run. For this reason, we modified the experimental setup.

Instead of fitting 100 reps, we fit three reps with three specific starting metadata balances: 25% snow, 50% snow, and 75% snow. These three metadata balances are chosen to represent cases starting with balanced data, those starting with majority snow images, and those starting with majority non-snow images, respectively. We also consider different comparator methods:

- **GPAML**: Our method as described in Section 2.
- **10% snow**: New images are selected at true proportion balance.
- **50% snow**: New images are selected at 50/50 rate.
- **All Snow**: All new images are snow images.
- **All Not Snow**: All new images are not snow images.

These methods are chosen in an attempt to control the variability of the experiment. We hope to capture the “best” and “worst” acquisition decisions by looking at the Snow and Not Snow competitors, since we assume one metadata category is more valuable to the ML model than the other. However, we also include comparators which choose some images from each metadata category: 50% snow, representing balanced metadata adds, and 10% snow, representing metadata added at the true proportion balance. The 10% snow comparator is chosen because we saw in the Spambase and MNIST experiments that the optimal proportion balance is often equal to the true proportion balance.

For the RarePlanes experiment we began with $N_{\text{start}} = 100$ images, and added $n = 50$ new images at a time until reaching size $N_{\text{stop}} = 1000$. For this experiment, we use F1 score to measure model accuracy. Out-of-sample of performance of the three reps is shown in Figure 7. The three panels show, from left to

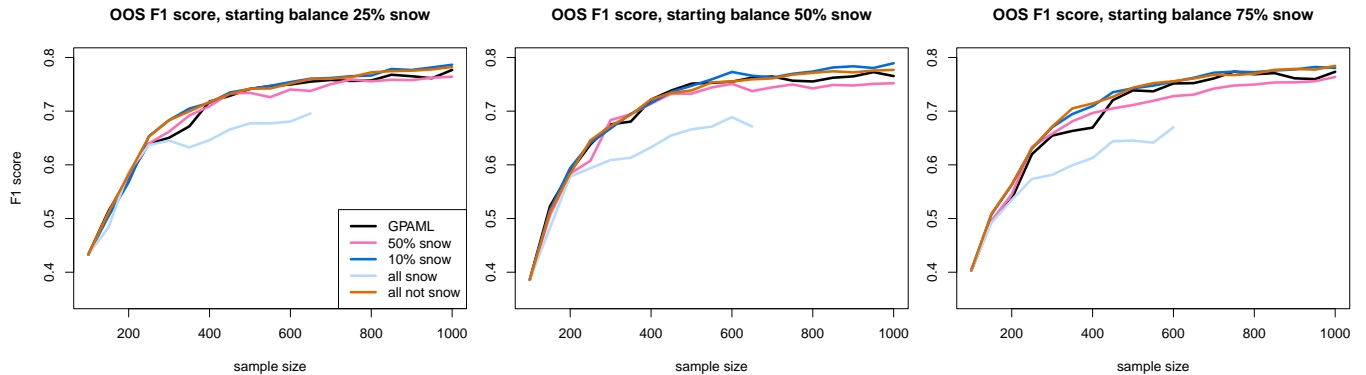


Figure 7: Out-of-sample performance for the 25% snow (left), 50% snow (center), and 75% snow (right) experiments.

right, the results of the 25% snow, 50% snow, and 75% snow starting metadata balances, respectively. We will comment on all three figures simultaneously since their results are similar.

For each of the three starting metadata balances, notice that out-of-sample model performance is roughly equivalent for all five competitors until size $N = 250$. Once reaching a size of $N = 250$, the Snow competitor begins to show much worse OOS performance than the other four competitors. This indicates that having a large proportion of Snow images is suboptimal, with this suboptimality worsening as the experiment continues. Moreover, note that the Snow method stops prior to our final size of $N_{\text{stop}} = 1000$ because we only have 600 Snow images available for D_N . The other four methods perform comparably to each other for most of the experiment, except for a bit of noise. However, only GPAML does not require pre-specified sampling proportions of the two metadata categories. We note that GPAML does not always make the optimal decision; note in particular the move from $N = 300$ to $N = 350$ in the 75% Snow experiment. We explore this suboptimality in Appendix B.

For additional perspective, Figure 8 shows the proportion balance for each of the three reps, relative to the Snow balance. They are shown in the same order as the previous plot. In each panel, a dashed line is

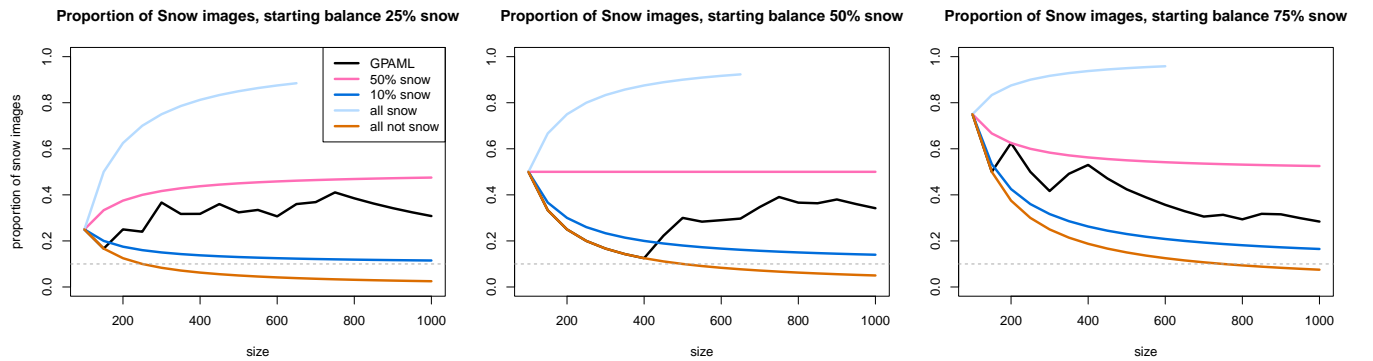


Figure 8: Proportion balances for the 25% snow (left), 50% snow (center), and 75% snow (right) experiments.

drawn horizontally at $y = 0.1$ to indicate the true proportion balance of Snow images. In these plots, the four non-GPAML competitors show smooth changes in proportion balance, since we add the same balance of images at each acquisition. So we focus on the results of GPAML. For each GPAML run, notice that GPAML prefers, but does not exclusively choose, data points from the Not Snow category. It is also able to self-correct after making a bad choice; in the 75% snow rep, it bounces between choosing lots of Snow and lots of Not Snow images, eventually settling on a path that selects primarily Not Snow images. These results match what we saw in the out-of-sample F1 results; that competitors with primarily Not Snow images performed better (All Not Snow, 10% snow). What is interesting is that the optimal proportion balance does not seem to be converging to the true 10% Snow balance; in all three cases, the ending Snow percentage is around 30%.

4 Discussion

We introduced a new idea for optimally selecting new data for ML models by considering the metadata associated with the data points to be added. We call this method GPAML, since we use a GP to learn the optimal metadata balance of new data points. We found that GPAML performs at least as well as (and in some cases better than) other data acquisition methods. In this scenario performing as well as other data

acquisition methods is suitable because other methods may also find the optimal metadata balance. Most importantly, GPAML protects against making data acquisitions that would hurt performance.

GPAML is restricted by the need to take subsamples from the existing data D_N . Because we asses the impact of metadata on model performance by taking subsamples from existing metadata categories, GPAML cannot estimate the impact of adding a data point from a new metadata category to the dataset. Additionally, if the number of data points in an existing metadata category is too small, it can be difficult for GPAML to estimate the impact of that category. Thus, for now we must begin with a dataset containing all metadata categories of interest, where the proportion balance is not extremely unbalanced.

One possible area for future work is to extend GPAML to metadata with more than two categories. The idea behind this is simple, although computational expense quickly increases. To train a GP for GPAML, we were considering $b = 100$ unique metadata balances in two dimensions. To get a suitable accuracy surface in higher dimension, we would likely need to take even more samples. Since each added rep requires fitting another ML model, the computational expense can quickly become unmanageable.

We are also interested in developing strategies that would mitigate the large computational cost of GPAML. We believe there may be a way to do this by selecting the training points $X^{(N)}$ for the GP in a more intelligent way. In particular, we want to develop a version of GPAML which reuses subsamples from previous iterations, so we do not need to fit 100 ML models at each iteration. One simple solution is to only collect new subsamples in the unexplored portions of the space. However, this would mean new images are never incorporated into the original space. We believe this idea could be modified by supplementing the new subsamples with a few additional subsamples in the original space, but exploring that idea represents future work.

A current shortcoming of this method is the assumption that we know the underlying proportion balance of the metadata, and using that as the proportion balance for the test set $D_{N_i}^{\text{test}}$. We made this decision after learning that random selection of the proportion selection of $D_{N_i}^{\text{test}}$ yielded suboptimal results. In particular, by choosing $D_{N_i}^{\text{test}}$ at random, its proportion balance (over many reps) converges to the proportion balance of D_N . We found that this can lead to a vicious cycle, where the current proportion balance is chosen as optimal for each acquisition; i.e., GPAML is not learning the true optimal metadata balance. We needed a way to avoid this vicious cycle. Assuming the underlying proportion balance is simple, but not always realistic. We would like to find a different way to specify the proportion balance of $D_{N_i}^{\text{test}}$ that does not rely on this assumption.

Acknowledgements

This material is based upon work supported, in whole or in part, by the U.S. Department of Defense, Director, Operational Test and Evaluation (DOT&E) through the Office of the Assistant Secretary of Defense for Research and Engineering (ASD(R&E)) under contracts HQ003419D0003 and HQ003424D0023. The Systems Engineering Research Center (SERC) is a federally funded University Affiliated Research Center managed by Stevens Institute of Technology. Any views, opinions, findings and conclusions or recommendations expressed in this material are those of the author(s) and do not necessarily reflect the views of the United States Department of Defense nor DOT&E nor ASD(R&E).

Declaration of Interest

The authors report no conflict of interest.

References

Abdelwahab, M. and Busso, C. (2019). Active learning for speech emotion recognition using deep neural network. In *2019 8th International conference on affective computing and intelligent interaction (ACII)*, pages 1–7. IEEE.

Abrahamsen, P. (1997). *A review of Gaussian random fields and correlation functions*. Norsk Regnesentral.

Angluin, D. (1988). Queries and concept learning. *Machine learning*, 2:319–342.

Ash, J. T., Zhang, C., Krishnamurthy, A., Langford, J., and Agarwal, A. (2019). Deep batch active learning by diverse, uncertain gradient lower bounds. *arXiv preprint arXiv:1906.03671*.

Baum, E. B. and Lang, K. (1992). Query learning can work poorly when a human oracle is used. In *International joint conference on neural networks*, volume 8, page 8. Beijing China.

Binois, M. and Gramacy, R. B. (2021). hetGP: Heteroskedastic Gaussian process modeling and sequential design in R. *Journal of Statistical Software*, 98(13):1–44.

Breiman, L. (2001). Random forests. *Machine learning*, 45:5–32.

Brinker, K. (2003). Incorporating diversity in active learning with support vector machines. In *Proceedings of the 20th international conference on machine learning (ICML-03)*, pages 59–66.

Cohn, D. (1993). Neural network exploration using optimal experiment design. *Advances in neural information processing systems*, 6.

Cortes, C. and Vapnik, V. (1995). Support-vector networks. *Machine learning*, 20:273–297.

Dagan, I. and Engelson, S. P. (1995). Committee-based sampling for training probabilistic classifiers. In *Machine learning proceedings 1995*, pages 150–157. Elsevier.

Fang, M., Li, Y., and Cohn, T. (2017). Learning how to active learn: A deep reinforcement learning approach. *arXiv preprint arXiv:1708.02383*.

Gramacy, R. B. (2020). *Surrogates: Gaussian process modeling, design, and optimization for the applied sciences*. CRC press.

Hoi, S. C., Jin, R., Zhu, J., and Lyu, M. R. (2006). Batch mode active learning and its application to medical image classification. In *Proceedings of the 23rd international conference on Machine learning*, pages 417–424.

Hopkins, Mark, R. E. F. G. and Suermondt, J. (1999). Spambase. UCI Machine Learning Repository. DOI: <https://doi.org/10.24432/C53G6X>.

Hospedales, T., Antoniou, A., Micaelli, P., and Storkey, A. (2021). Meta-learning in neural networks: A survey. *IEEE transactions on pattern analysis and machine intelligence*, 44(9):5149–5169.

Hsu, W.-N. and Lin, H.-T. (2015). Active learning by learning. In *Proceedings of the AAAI Conference on Artificial Intelligence*, volume 29.

Irizarry, R. A. and Gill, A. (2024). *dslabs: Data Science Labs*. R package version 0.8.0.

Jones, D. R., Schonlau, M., and Welch, W. J. (1998). Efficient global optimization of expensive black-box functions. *Journal of Global optimization*, 13:455–492.

Konyushkova, K., Sznitman, R., and Fua, P. (2017). Learning active learning from data. *Advances in neural information processing systems*, 30.

Lanus, E., Lee, B., Pol, L., Sobien, D., Kauffman, J., and Freeman, L. J. (2024). Coverage for identifying critical metadata in machine learning operating envelopes. In *2024 IEEE International Conference on Software Testing, Verification and Validation Workshops (ICSTW)*, pages 217–226.

LeCun, Y. (1998). The MNIST database of handwritten digits. <http://yann. lecun. com/exdb/mnist/>.

LeCun, Y., Bottou, L., Bengio, Y., and Haffner, P. (1998). Gradient-based learning applied to document recognition. *Proceedings of the IEEE*, 86(11):2278–2324.

Lewis, D. D. (1995). A sequential algorithm for training text classifiers: Corrigendum and additional data. In *Acm Sigir Forum*, volume 29, pages 13–19. ACM New York, NY, USA.

Lewis, D. D. and Gale, W. A. (1994). A sequential algorithm for training text classifiers. In *Proceedings of the ACM SIGIR Conference on Research and Development in Information Retrieval*, pages 3–12. ACM New York, NY, USA.

Liaw, A. and Wiener, M. (2002). Classification and regression by randomForest. *R News*, 2(3):18–22.

MacKay, D. J. (1992). Information-based objective functions for active data selection. *Neural computation*, 4(4):590–604.

Olsson, F. (2009). A literature survey of active machine learning in the context of natural language processing.

Paszke, A., Gross, S., Massa, F., Lerer, A., Bradbury, J., Chanan, G., Killeen, T., Lin, Z., Gimelshein, N., Antiga, L., et al. (2019). PyTorch: An imperative style, high-performance deep learning library. In *Advances in Neural Information Processing Systems*, volume 32, pages 8024–8035.

Picheny, V., Gramacy, R. B., Wild, S., and Le Digabel, S. (2016). Bayesian optimization under mixed constraints with a slack-variable augmented lagrangian. *Advances in neural information processing systems*, 29.

Rasmussen, C. E. and Williams, C. K. (2006). *Gaussian processes for machine learning*, volume 2. MIT press Cambridge, MA.

Redmon, J., Divvala, S., Girshick, R., and Farhadi, A. (2016). You only look once: Unified, real-time object detection. In *Proceedings of the IEEE conference on computer vision and pattern recognition*, pages 779–788.

Ren, P., Xiao, Y., Chang, X., Huang, P.-Y., Li, Z., Gupta, B. B., Chen, X., and Wang, X. (2021). A survey of deep active learning. *ACM computing surveys (CSUR)*, 54(9):1–40.

Rosenblatt, F. (1958). The perceptron: a probabilistic model for information storage and organization in the brain. *Psychological review*, 65(6):386.

Roy, N. and McCallum, A. (2001). Toward optimal active learning through sampling estimation of error reduction. In *In Proc. 18th International Conf. on Machine Learning*.

Rumelhart, D. E., Hinton, G. E., and Williams, R. J. (1986). Learning representations by back-propagating errors. *nature*, 323(6088):533–536.

Sacks, J., Welch, W., Mitchell, T., and Wynn, H. (1989). Design and analysis of computer experiments. *Statistical Science*, (4).

Santner, T. J., Williams, B. J., Notz, W. I., and Williams, B. J. (2003). *The design and analysis of computer experiments*, volume 1. Springer.

Seo, S., Wallat, M., Graepel, T., and Obermayer, K. (2000). Gaussian process regression: Active data selection and test point rejection. In *Mustererkennung 2000: 22. DAGM-Symposium. Kiel, 13.–15. September 2000*, pages 27–34. Springer.

Settles, B. (2009). Active learning literature survey. Computer Sciences Technical Report 1648, University of Wisconsin–Madison.

Settles, B., Craven, M., and Ray, S. (2007). Multiple-instance active learning. *Advances in neural information processing systems*, 20.

Seung, H. S., Opper, M., and Sompolinsky, H. (1992). Query by committee. In *Proceedings of the fifth annual workshop on Computational learning theory*, pages 287–294.

Shermeyer, J., Hossler, T., Van Etten, A., Hogan, D., Lewis, R., and Kim, D. (2021). RarePlanes: Synthetic data takes flight. In *Proceedings of the IEEE/CVF Winter Conference on Applications of Computer Vision*, pages 207–217.

Snoek, J., Larochelle, H., and Adams, R. P. (2012). Practical bayesian optimization of machine learning algorithms. *Advances in neural information processing systems*, 25.

Stein, M. L. (1999). *Interpolation of spatial data: some theory for kriging*. Springer Science & Business Media.

Torres, R. N., Fraternali, P., and Romero, J. (2020). Odin: An object detection and instance segmentation diagnosis framework. In *European Conference on Computer Vision*, pages 19–31. Springer.

Ultralytics (2023). YOLOv8 [Software]. <https://github.com/ultralytics/ultralytics>.

Vilalta, R. and Drissi, Y. (2002). A perspective view and survey of meta-learning. *Artificial intelligence review*, 18(2):77–95.

Willemink, M. J., Koszek, W. A., Hardell, C., Wu, J., Fleischmann, D., Harvey, H., Folio, L. R., Summers, R. M., Rubin, D. L., and Lungren, M. P. (2020). Preparing medical imaging data for machine learning. *Radiology*, 295(1):4–15.

Wood, J. (2024). *RcppAlgos: High Performance Tools for Combinatorics and Computational Mathematics*. R package version 2.8.5.

Yang, Y., Ma, Z., Nie, F., Chang, X., and Hauptmann, A. G. (2015). Multi-class active learning by uncertainty sampling with diversity maximization. *International Journal of Computer Vision*, 113(2):113–127.

Yin, C., Qian, B., Cao, S., Li, X., Wei, J., Zheng, Q., and Davidson, I. (2017). Deep similarity-based batch mode active learning with exploration-exploitation. In *2017 IEEE international conference on data mining (ICDM)*, pages 575–584. IEEE.

Zhu, X., Zhang, P., Lin, X., and Shi, Y. (2007). Active learning from data streams. In *Seventh IEEE International Conference on Data Mining (ICDM 2007)*, pages 757–762. IEEE.

Žliobaitė, I., Bifet, A., Pfahringer, B., and Holmes, G. (2013). Active learning with drifting streaming data. *IEEE transactions on neural networks and learning systems*, 25(1):27–39.

SUPPLEMENTARY MATERIAL

A Metadata Preprocessing

In order for a metadata category to be suitable for GPAML, or any other metadata-based acquisition strategy, that category needs to have a meaningful impact on model performance. Here we demonstrate that our chosen metadata variables are expected to have an impact on performance.

A.1 Spambase

For the Spambase dataset we used metadata separating emails into those with no special characters, and those with at least one special character. To check whether this metadata affects model performance we performed a simple experiment comparing datasets comprised primarily of emails with no special characters to datasets comprised primarily of emails with at least one special character. In particular, for each metadata category, we randomly selected 90 emails from that metadata category, and 10 emails from the other metadata category. We then evaluated this dataset on a holdout set of 500 emails. This was repeated 100 times for each metadata category, creating the boxplot in the left panel of Figure 9. Here we

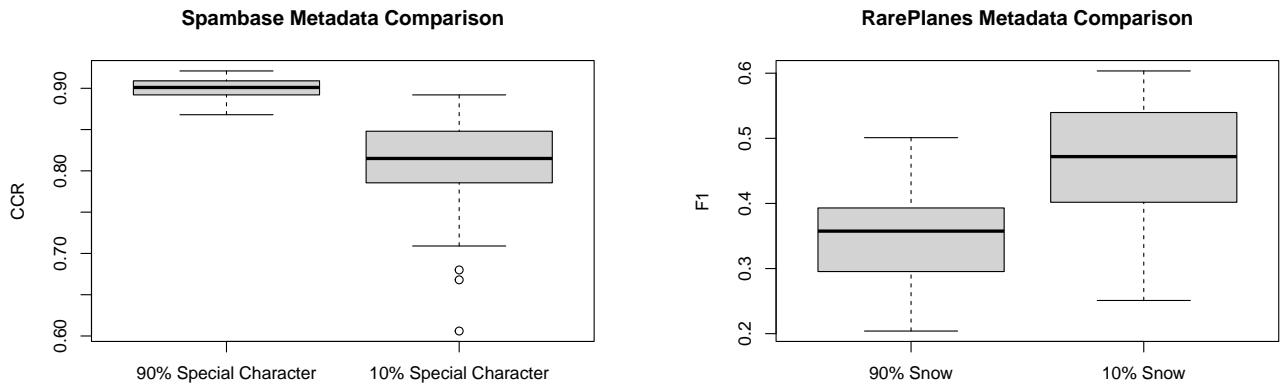


Figure 9: *Left:* OOS CCR for Spambase metadata comparison; *right:* OOS F1 score for RarePlanes metadata comparison.

see that, in general, it is beneficial to collect emails with at least one special character. Since there is a difference in model performance for each metadata category, it is suitable for GPAML.

A.2 MNIST

For the MNIST dataset, we used metadata which separated digits into those easy to categorize and those difficult to categorize. By looking at confusion matrices comparing the true and predicted digits for a single run of the NN, we can learn which MNIST digits are easy and difficult to categorize. We looked at the confusion matrices produced by several runs of the model to learn: (i) digits that are easy and difficult to categorize and (ii) digits that are frequently confused with each other. An example of a confusion matrix is shown in 10. From this plot, we can learn which digits are frequently misclassified, and which are frequently predicted incorrectly. We attempt to summarize these two pieces of information (i.e., the final row and column of the confusion matrix), grouping together digits that are frequently confused with each other. Summarizing all this information, we placed digits 0, 1, 4, 5, 6, and 7 and in the easy category, and digits 2, 3, 8, and 9 in the hard category.

	0	1	2	3	4	5	6	7	8	9	CCR
0	92	0	2	1	0	2	2	0	1	3	0.89
1	0	113	1	0	0	0	0	0	0	0	0.99
2	0	2	65	0	5	0	2	4	1	9	0.74
3	0	1	5	74	0	4	1	4	9	2	0.74
4	0	1	0	0	89	1	0	0	9	3	0.86
5	0	1	0	19	4	47	5	2	10	6	0.5
6	1	2	1	3	8	0	71	0	0	1	0.82
7	0	1	3	0	0	2	0	96	3	17	0.79
8	0	2	2	2	0	5	0	1	93	3	0.86
9	0	0	0	2	11	4	0	10	11	43	0.53
CCR	0.99	0.92	0.82	0.73	0.76	0.72	0.88	0.82	0.68	0.49	

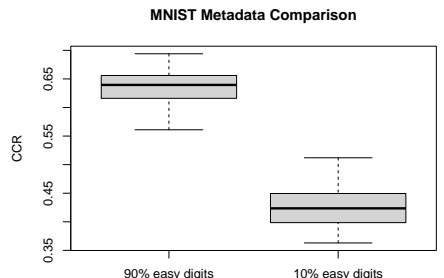


Figure 10: *Left:* Confusion matrix for a single rep of the MNIST experiment; *right:* OOS CCR for MNIST metadata comparison.

To double check that we have created metadata suitable for GPAML, we performed an experiment similar to that in Section A.1. In particular, for each metadata category we randomly selected 90 images from that metadata category and 10 images from the opposite category. The model performance was evaluated on a holdout set of 1000 images. We repeated this process 100 times for each metadata category to create the boxplot in the right panel of Figure 10.

A.3 RarePlanes

For the RarePlanes dataset we used metadata describing the weather in which an image was taken: snowy, or not snowy. To see whether this metadata affects model performance we performed an experiment similar to the one in Section A.1. In particular, for each metadata category, we randomly selected 90 images from that metadata category and 10 images from the opposite category. The model performance was evaluated on a holdout set of 1000 images. This process was repeated 100 times for each metadata category, creating the boxplot in the right panel of Figure 9. Here we see that, in general, it is beneficial to collect more images in the Not Snow category. This difference in model performance makes it suitable for GPAML.

B Effect of different samples

The choice of optimal metadata balance by GPAML depends on the subsamples selected during the metadata balance varying experiment. To explore this further, we look at the impact of different subsamples at one acquisition of the RarePlanes experiment. In particular, we explore the experiment starting with 75% Snow and look at the move from $N = 300$ to $N = 350$. We chose this move because GPAML suddenly underperforms its competitors (see Figure 7). This is caused by selecting primarily Snow images (see Figure 8), which is a suboptimal decision. We complete a simple experiment to explore the effect of subsamples on the acquisition decision. Instead of our typical $b = 100$ unique metadata balances chosen, we simulated a total of $b = 250$ unique metadata balances; this includes the 100 subsamples selected in the original experiment.

From this collection of unique metadata balances, we designed three experiments to explore the effect of sample collection on the decision made by GPAML. In particular, from these $b = 250$ unique metadata balances, we took random samples of sizes 100, 150, and 200, and used the selected samples to fit the GP. We took 100 random samples for each sample size. The acquisition decision line for each GP is shown in Figure 11 for samples of sizes 100, 150, and 200, from left to right. In this figure, we plot the integrated

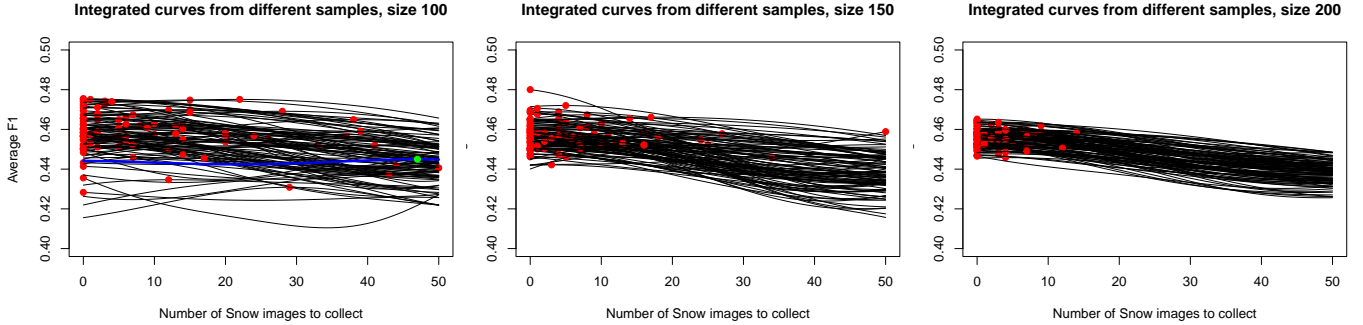


Figure 11: Integrated GPAML curve from 100 random samples of points. Acquisition choices are shown as red dots. The blue line shows our original acquisition line, with a green point denoting the original acquisition decision.

model performance learned from each GP as a black line, with a red dot denoting the acquisition decision. We also include the original sample of size 100 (i.e., the one shown in Figures 7 and 8) as a blue line, with a green dot denoting the acquisition decision.

From the results in Section 3.3, we learned that in general, any acquisition decision that chooses a majority of Not Snow images is a good decision. Using this criterion, we see that GPAML makes a good decision around 90% of the time with samples of size 100, around 98% of the time for size 150, and 100% of the time for size 200. It is unsurprising that collecting more samples provides more consistent results. However, given the extra computational cost of collecting 50 more samples, we are satisfied with a method that makes the correct decision 90% of the time. We also note that the sub-optimal decision which originally interested us was a particularly unlucky decision; only four other samples of size 100 made a decision as bad or worse. We also note that, although GPAML made a bad decision at size $N = 300$, it was able to correct itself in the next step, at $N = 350$.